ChemComm

Consequences of Substituting Framework Metals in Polyoxometalates on H-atom Uptake: Proton-coupled Electron Transfer at a Keggin-type Polyoxomolybdate

Journal:	*ChemComm*
Manuscript ID	CC-COM-04-2025-001894.R1
Article Type:	Communication

ChemComm

COMMUNICATION

Consequences of Substituting Framework Metals in Polyoxometalates on H-atom Uptake: Proton–Coupled Electron Transfer at a Keggin-type Polyoxomolybdate

Received 00th January 20xx,
Accepted 00th January 20xx

DOI: 10.1039/x0xx00000x

Zhou Lu and Ellen M. Matson*[a]

The proton–coupled electron transfer to the surface of a Keggin-type polyoxomolybdate, $[^nBu_4N]_3[PMo_{12}O_{40}]$, is described. The thermochemistry of surface O–H bonds generated upon reduction/protonation of the assembly is determined (~67 kcal mol^{-1}). Kinetic investigations provide evidence that proton–electron pairs are added to the polyoxomolybdate surface through a concerted mechanism.

Polyoxometalates (POMs) are molecular assemblies that consist of multiple redox-active transition metal oxyanions linked together by bridging oxide units to form three dimensional structures.[1,2] One of the most advantageous features of POMs is their ability to perform reversible charge transfer reactions.[2,3] The modular character of these molecular metal oxides allows for extensive tuning of both the number of redox events, as well as the electrochemical potential of reduction.[4–6] In addition to structural modifications that influence the physicochemical properties of POMs, the electrochemistry of these metal oxide assemblies have been shown to be sensitive to the identity of charge compensating counter ions in solution. For instance, alkali ions have been shown to interact strongly with the surface of POMs, resulting in a positive shift in the reduction potentials of the assembly.[7] Additional studies have focused on the ability of POMs to interact with protons as a function of charge state.[8]

The differences in redox thermochemistry of POMs in acidic and neutral environments are often significant.[2,9] In the absence of protons, most POMs exhibit multiple single electron reduction events. Addition of acid results in anodic shifts; in some cases, individual redox events appear to merge into multielectron-multiproton reduction processes. This phenomenon is broadly indicative of proton–coupled electron transfer. Indeed, studies from our group reveal that a subset of POMs, namely Keggin-type polyoxotungstate (POT) clusters, $[EW_{12}O_{40}]^{3-}$ (E = P[10], V[11]), form surface O–H bonds upon reduction in the presence of acid. Given the low reduction potential and the surface acidity of $[EW_{12}O_{40}]^{3-}$, the resultant O–H bonds are quite weak, with bond dissociation free energies (BDFEs) ranging from 42-48 kcal mol^{-1}.[10,11] While these POTs are poised to serve as electrocatalysts for hydrogenation chemistries, their low BDFE(O–H) value can result in competitive hydrogen production (BDFE(H–H) = 51 kcal/mol in acetonitrile),[12] which may limit faradaic efficiency and selectivity.

Polyoxomolybdates (POMos) constitute an additional class of POMs. In many examples, the composition and structure of POMos mirror that of their tungstate analogues (e.g. $[PW_{12}O_{40}]^{3-}$ (**PW_{12}**) vs. $[PMo_{12}O_{40}]^{3-}$ (**PMo_{12}**)); both metals are Group(VI) ions that adopt hexavalent oxidation states (**Fig. 1**). However, POMos are more easily reduced and basic in comparison to their POT derivatives.[13] These changes in the properties (e.g. $E_{1/2}$, pK_a) of the assembly observed as a result of swapping the framework metals should have a substantial impact on the thermochemistry of H-atom uptake reactions.

Given the established discrepancies in reduction potential and basicity between POTs and POMos, we became interested in understanding the thermochemistry of H-atom uptake in molecular molybdenum oxide assemblies. Limited investigations into the PCET reactivity of these clusters have been reported as a result of their tendency to undergo hydrolysis or other rearrangement reactions in water.[14,15] Our focus on the nonaqueous chemistry of POMs presents an opportunity to study these systems by inhibiting/limiting structural rearrangements that complicate analyses.

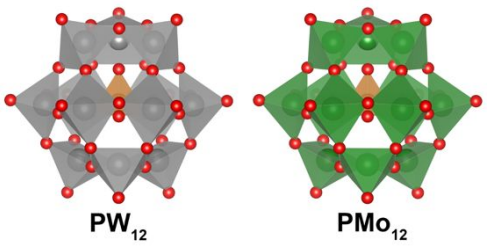

Fig. 1. Molecular structures of Keggin-type POMs investigated in this work. Structures are generated from publicly accessible CIF files (**PW_{12}** = MUWZIO[30]; **PMo_{12}** = EBUKIW[31]), and omit counter cations and solvent molecules for clarity. KEY: Red spheres = O; Orange polyhedra = P; Green polyhedra = Mo; grey polyhedra = W.

[a] *Department of Chemistry, University of Rochester, Rochester NY 14627, USA.*
Electronic Supplementary Information (ESI) available: Experimental procedures, cyclic voltammograms, open circuit potential analyses, kinetic data for mechanistic studies. See DOI: 10.1039/x0xx00000x

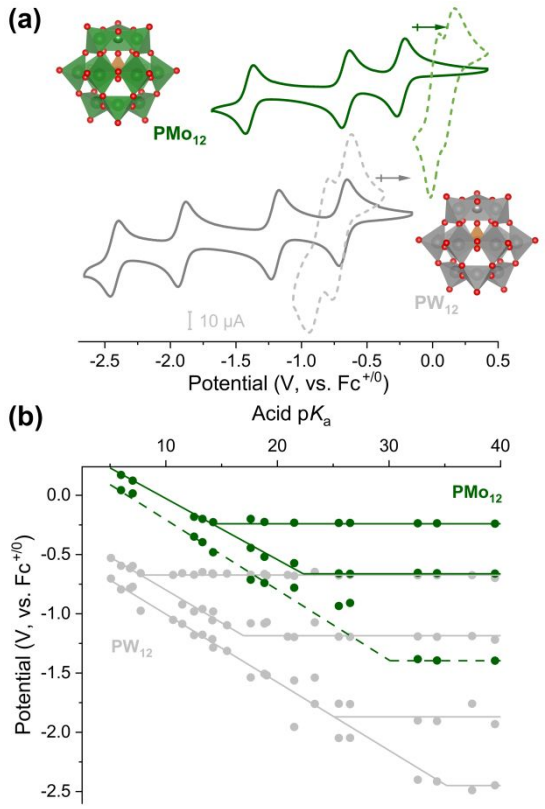

Fig. 2. (a) Cyclic voltammograms (CVs) of 1 mM of **PMo_{12}** (green) and **PW_{12}** (grey) in the absence of acids (solid lines) and in the presence of 4 mM 2-Bromo-pyridinium tetrafluoroborate (2-Br-PyrHBF$_4$, pK_a = 7.02, dashed lines) obtained in MeCN with 0.1 M TBAPF$_6$ as the supporting electrolyte (100 mV/s). The CV of **PMo_{12}** at highly negative potentials shows quasi-reversible redox processes in the presence of acid, however we have concerns about the reliability of the pK_a dependent data due to the instability of **PMo_{12}** under these conditions (see green-dashed line in **Fig. 2b**); (b) Potential-pK_a diagram of **PMo_{12}** (green) and **PW_{12}** (grey). Each data point represents an individual CV collected using 1 mM of cluster and 4 mM of organic acid in MeCN. The potentials were calibrated using $Fc^{+/0}$ as the internal standard.

The cyclic voltammogram (CV) of **PMo_{12}** in acetonitrile exhibits three reversible reduction events ($E_{1/2}$ = -0.24, -0.66, and -1.40 V vs. $Fc^{+/0}$; **Fig. 2**). This is one fewer reduction event than is observed in the case of **PW_{12}** as a result of the instability of reduced variants of the POMo.[16] Notably, the redox events of **PMo_{12}** are shifted from that of **PW_{12}** by approximately +0.45 V.[17] The anodic shift in reduction processes in the case of **PMo_{12}** is credited to an increase in relativistic effects for tungsten as a result of its increased nuclear charge per unit volume.[13] Upon adding an excess of the acids, these separate redox events collapse into two multielectron redox shift with positive shift, as indicated in **Fig. 2a** using 2-Br-PyrHBF$_4$ as an example.

To determine the thermochemistry of H-atom uptake at the surface of **PMo_{12}**, electrochemical measurements of the POMo were performed in the presence of a series of organic acids (4 equiv) with pK_a values ranging from 10-38 (Fig. S1, see ESI for additional details).[18] Plotting the reduction potential ($E_{1/2}$) vs. the pK_a of the added organic acid results in the construction of a potential-pK_a diagram for **PMo_{12}** (**Fig. 2b**). In the presence of organic acids with pK_a values > 30, no changes were observed in the redox events. The use of moderate acids (pK_a values < 28) results in the shift of the most negative reduction event. Notably, this redox process appears irreversible in the presence of moderate acids as a result of the lability of the POMo in the presence of organic acids and strong reductants as reported.[19] Given this instability, we focused our attention on proton-dependence of the first two reduction processes of **PMo_{12}**.

The addition of stronger organic acids (pK_a < 22) to **PMo_{12}** results in the anodic shift of the event originating at -0.66 V. This feature combines with the most positive redox event into a $2e^-/2H^+$ process in the presence of organic acids with pK_a values < 15. The observed shifts in $E_{1/2}$ of **PMo_{12}** in the presence of the selected organic acids indicate that electron transfer to the cluster is coupled to proton transfer under appropriate conditions. Best fits of proton–dependent regions give slopes of 53 mV/pK_a unit, close to the Nernstian value of 59 mV/pK_a unit expected for an n-electron, n-proton processes (*i.e.*, 1:1 ratio of protons and electrons). Locating the intersections of acid dependent and independent regions of the diagram results in acid dissociation constants of 22.3±1.0 (pK_a2), and 14.1±0.5 (pK_a1) for the reduced and protonated clusters (see Eq 1-2).

pK_a1: $[PMo_{12}O_{39}(OH)]^{3-} \rightleftharpoons [PMo_{12}O_{40}]^{4-} + H^+$ Eq. 1

pK_a2: $[PMo_{12}O_{38}(OH)_2]^{3-} \rightleftharpoons [PMo_{12}O_{39}(OH)]^{4-} + H^+$ Eq. 2

The experimentally obtained pK_a values of the reduced and protonated forms of **PMo_{12}** are higher than those measured for **PW_{12}**. This result confirms that the POMo has a higher affinity for protons than the POT, a point further supported by density functional theory (DFT) calculations (**Fig. 3**). The lowest unoccupied molecular orbitals (LUMO) were plotted for two clusters (**Fig. 3a-b**); in the case of **PW_{12}**, the reducing equivalent is located primarily at metal sites (82.3%W vs. 17.7%O character), while in **PMo_{12}**, the LUMO extends to bridging oxide ligands (75.5%Mo vs. 24.5%O character). These data support increased basicity of the bridging oxide sites of **PMo_{12}** upon reduction. Mapping out the electrostatic potential (ESP) reveals an electron-rich region located around M_4O_{b4} pocket in both assemblies, with a higher concentration of electron density in **PMo_{12}** in comparison to **PW_{12}** (**Fig. 3c-3d**, Fig. S2).[20]

With the reduction potential and pK_a values of the reduced

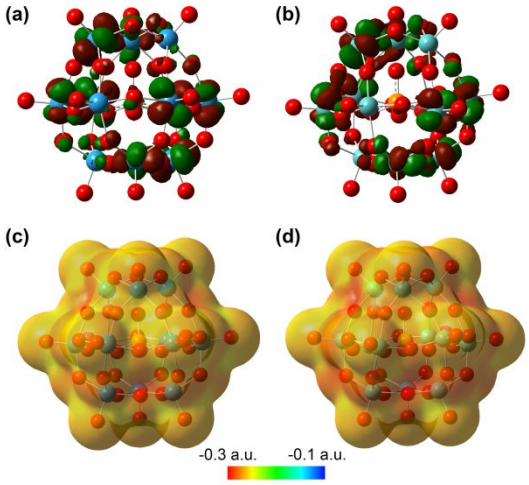

Fig. 3. Graphical summary of DFT results. LUMOs of (a) **PW_{12}** and (b) **PMo_{12}** (isovalue = 0.03 a.u.). (b) Electrostatic potential (ESP) maps of (c) **PW_{12}** and (d) **PMo_{12}** at the iso-electron-density surface of 0.002 a.u.

forms of **PMo_{12}** in hand, the BDFE(O–H) values of surface hydroxyl groups in the reduced POMo assembly can be determined using the Bordwell equation:

$$BDFE(E–H) = 1.37pK_a + 23.06E^0 + C_g \quad \text{Eq 3}$$

where pK_a and E^0 are the acid dissociation and reduction potentials collected experimentally and C_g is a constant associated with the H^+/H in the reference solvent (for acetonitrile, C_g = 52.6 kcal mol^{-1}). The average BDFE(O–H) value of 67.2 ± 1.0 kcal mol^{-1} (Eqn 4) was determined for the reduced and protonated forms of **PMo_{12}**.

$$BDFE(O–H)_{avg}: [PMo_{12}O_{38}(OH)_2]^{3-} \rightleftharpoons [PMo_{12}O_{40}]^{3-} + 2H^+ + 2e^- \quad \text{Eq.4}$$

It should be noted that only the average BDFE value of two O–H bonds is presented, as we are unable isolate the monoreduced, monoprotonated assembly (*vide infra*).

The $BDFE(O\text{-}H)_{avg}$ value determined for **PMo_{12}** is substantially stronger than those reported for previously by our research group for the analogous Keggin-type POT ion, **PW_{12}** ($BDFE(O–H)_{avg}$ = 48.1, 43.7 kcal mol^{-1}).[10] The trends in the thermodynamics of the O–H bonds formed at the surface of reduced Keggin-type clusters are also consistent with observations made for extended solids (i.e., MoO_3 in comparison to WO_3). For example, the investigation of electrochemical proton transport in Group(VI) oxides reveals that the hydrogen evolution reaction is less favourable in MoO_3, suggesting a thermodynamic preference for H-atom adsorption rather than dissociation.[21] MoO_3 was further demonstrated to be capable of adsorbing more H-atoms via hydrogen spillover than WO_3 under identical reaction conditions.[22]

The $BDFE(O–H)_{avg}$ predicted for the reduced and protonated assembly, $[PMo_{12}O_{38}(OH)_2]^{3-}$ (**$2e^-/2H^+$-PMo_{12}**), suggests it will be resistant to hydrogen evolution (BDFE(H–H) = 51.2 kcal mol^{-1}, ΔG = +16 kcal mol^{-1}) and therefore isolable.[12,23] To isolate the relevant reduced and protonated form of the assembly, we opted to investigate the reactivity of hydrazobenzene (H_2Azo, BDFE(O–H) = 60.9 kcal mol^{-1} in acetonitrile[24]) with **PMo_{12}**. Addition of an excess of H_2Azo (2 equiv) to **PMo_{12}** results in a colour change from yellow to dark cyan. Characterization of the cyan product by ^{31}P NMR spectroscopy reveals a single resonance at 3.9 ppm; we note that this signal is observed at the similar chemical shift for the two-electron reduced assembly, $[PMo_{12}O_{40}]^{5-}$ (**$2e^-$-PMo_{12}**; 4.2 ppm), independently synthesized by addition of multiple equivalents of cobaltocene (Fig. S4 and see ESI for details of synthetic procedure). Further characterization of the cyan powder was performed via electronic absorption spectroscopy (Fig. S7). The oxidized assembly, **PMo_{12}**, exhibits only a single intense absorption at 308 nm (ε = 23090 M^{-1} cm^{-1}) assigned to ligand–to–metal charge transfer (LMCT, O_{yl}→Mo); upon hydrogenation, the LMCT band shifts by 10 nm and a new feature originating from intervalence charge transfer (IVCT, Mo^{IV}→Mo^{V}) emerges at 747 nm (ε = 3540 M^{-1} cm^{-1}). This transition matches that observed in solutions of **$2e^-$-PMo_{12}** (λ = 747 nm, ε = 3540 M^{-1}), consistent with similar degrees of reduction of the assembly. Titrations of **$2e^-/2H^+$-PMo_{12}** with 2,4,6-^{t}Bu$_3$PhO$^\bullet$ radical confirm the stoichiometry of H-atom uptake at **PMo_{12}** (Figs. S5-S6). Further evidence for the formation of the $2e^-/2H^+$ reduced cluster is obtained through open circuit potential analyses; the OCP of ratios of [**PMo_{12}**]/[**$2e^-/2H^+$-PMo_{12}**] were plotted as a function of concentration gradient, revealing a slope of 25.7 ± 0.6 mV dec^{-1}, consistent with a $2e^-$ process (Fig S9, see ESI for details).[25]

Having confirmed formation of **$2e^-/2H^+$-PMo_{12}**, our interests shifted to understanding the mechanism of PCET to **PMo_{12}**. Kinetic studies were performed through a series of pseudo first order analyses. As described above, the addition of H_2Azo to **PMo_{12}** acetonitrile solution results in the growth of the IVCT band at ~750 nm, consistent with the formation of **$2e^-/2H^+$-PMo_{12}** (**Fig. 4**). Extraction of the pseudo first-order rate constant is accomplished by exponentially fitting the increase in concentration of the reduced cluster. A plot of k_{obs} against the concentration of H_2Azo reveals a linear correlation, suggesting the reaction is first order with respect to substrate (**Fig. 4b**). The rate constant for H-atom uptake at **PMo_{12}** ($k_{PCET\text{-}H}$) can be found from the slope in **Fig. 4b**, where $k_{PCET\text{-}H}$ is equal to 1/24 *slope of the best fit line to account for the number of bridging oxide atoms available for H-atom uptake ($k_{PCET\text{-}H}$ = 0.10 ± 0.007 M^{-1} s^{-1} at 273 K). We note that the units of the rate constant are

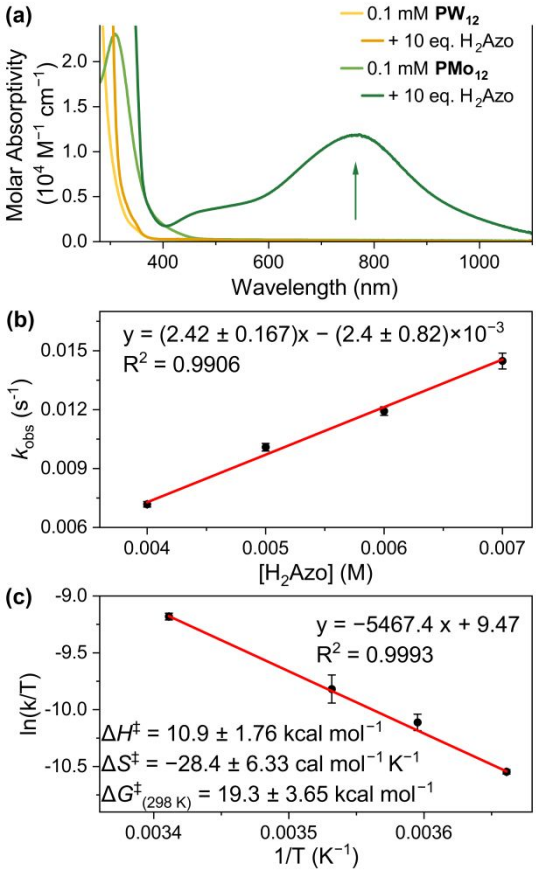

Fig. 4. (a) Electronic absorption spectra of 0.1 mM (yellow) **PW_{12}** and (green) **PMo_{12}** before and after adding ten equivalents of H_2Azo. (b) Plot of k_{obs} as a function of [H_2Azo] with the concentration of **PMo_{12}** held constant at 0.125 mM at 0 °C. The concentration of H_2Azo is varied between 4 and 7 mM. (c) Eyring plot of the reaction of **PMo_{12}** (0.125 mM) and H_2Azo (4 mM) in MeCN between 0 and 20 °C. The *Y*-axis adapts k_{obs} values.

consistent with a second-order process, indicating that the H-atom transfer is first-order H_2Azo (donor) and **PMo_{12}** (acceptor). Kinetic analysis using deuterium labelled substrate (D_2Azo) yields a kinetic isotope effect (KIE) of 2.2 (Fig. S14–S17). Collectively, these experiments suggest that the formation of **$2e^-/2H^+$-PMo_{12}** occurs through a rate limiting step of proton-coupled electron transfer from H_2Azo to **PMo_{12}**.

Eyring analysis of the H-atom transfer reaction from H_2Azo to **PMo_{12}** was performed to gain additional insight into the mechanism of PCET to the surface of the cluster (**Fig. 4c**, Fig. S18-S20). Our group and others have demonstrated that the nature of the transition state of H-atom transfer can differentiate between concerted and step-wise mechanisms of PCET.[26,27] We measured k_{obs} under pseudo-first order reaction conditions across a range of temperatures (0-20 °C). to determine the activation parameters for the rate-limiting H-atom transfer step. The $\Delta H^{\ddagger}$ (10.9 kcal mol^{-1}) and $\Delta S^{\ddagger}$ (-28.4 cal mol^{-1} K^{-1}) values are comparable to those reported for *concerted* PCET reactions at the surface of polyoxometalates.[11,28,29] The small magnitude of $\Delta H^{\ddagger}$ and large negative value for $\Delta S^{\ddagger}$ can be explained by the fact that the cluster engages in strong hydrogen bonding interactions with the substrate.

In summary, we establish the proton–coupled electron transfer reactivity of **PMo_{12}** in organic media and highlight the similar acid-dependent charge transfer behaviour of the Keggin-type clusters. Experimental evaluation of the strength of surface O–H bonds in the reduced and protonated assembly, **$2e^-/2H^+$-PMo_{12}**, reveal a BDFE(O-H)$_{avg}$ value of 67.2 ± 1.0 kcal mol^{-1}. We note that this value constitutes an increase in BDFE by ~20 kcal mol^{-1} for over its tungsten. We attribute this observed change in thermochemistry of H-atom uptake for the POMo to the increased basicity and reducibility of the molybdenum oxide assembly. Kinetic analyses with H-atom donor H_2Azo reveals a concerted proton-electron transfer mechanism.

Financial support of this work was provided by the Department of Energy under Award No. DE-SC0023465.

Data availability

The experimental data supporting this article have been included as part of the ESI.

Conflicts of interest

There are no conflicts to declare.

Notes and references

1 N. I. Gumerova and A. Rompel, *Chem. Soc. Rev.*, 2020, **49**, 7568–7601.
2 N. I. Gumerova and A. Rompel, *Nat. Rev. Chem.*, 2018, **2**, 0112.
3 L. Yang, J. Lei, J. Fan, R. Yuan, M. Zheng, J. Chen and Q. Dong, *Adv. Mater.*, 2021, **33**, e2005019.
4 K. Nakajima, K. Eda and S. Himeno, *Inorg. Chem.*, 2010, **49**, 5212–5215.
5 K. Maeda, H. Katano, T. Osakai, S. Himeno and A. Saito, *J. Electroanal. Chem.*, 1995, **389**, 167–173.
6 T. McCormac, B. Fabre and G. Bidan, *J. Electroanal. Chem.*, 1997, **425**, 49–54.
7 (a) M. Pascual-Borràs, E. Arca, H. Yoshikawa, T. Penfold, P. G. Waddell and R. J. Errington, *J. Am. Chem. Soc.*, 2024, **146**, 26485–26496. (b) J.-J. Chen, M. D. Symes and L. Cronin, *Nat. Chem.*, 2018, **10**, 1042–1047. (c) A. Misra, K. Kozma, C. Streb and M. Nyman, *Angew. Chem. Int. Ed.,* 2020, **59**, 596–612.
8 (a) E. Schreiber, W. W. Brennessel and E. M. Matson, *Inorg. Chem.*, 2022, **61**, 4789–4800. (b) J. Nambu, T. Ueda, S.-X. Guo, J. F. Boas and A. M. Bond, *Dalton Trans.*, 2010, **39**, 7364–7373. (c) P. J. S. Richardt, R. W. Gable, A. M. Bond and A. G. Wedd, *Inorg. Chem.*, 2001, **40**, 703–709. (d) T. Ueda, J. Nambu, J. Lu, S.-X. Guo, Q. Li, J. F. Boas, L. L. Martin and A. M. Bond, *Dalton Trans.*, 2014, **43**, 5462–5473.
9 T. Ueda, *ChemElectroChem*, 2018, **5**, 823–838.
10 Z. Lu, S. E. Cooney, J. R. McKone and E. M. Matson, *JACS Au*, 2024, **4**, 1310–1314.
11 Z. Lu, M. Dagar, J. R. McKone and E. Matson, *Chem. Sci.*, DOI:10.1039/d4sc08452g.
12 J. J. Warren, T. A. Tronic and J. M. Mayer, *Chem. Rev.*, 2010, **110**, 6961–7001.
13 A. Döring and C. Schulzke, *Dalton Trans.*, 2010, **39**, 5623–5629.
14 N. I. Gumerova and A. Rompel, *Sci. Adv.*, 2023, **9**, eadi0814.
15 M. J. D. Silva and M. G. Teixeira, *RSC Adv.*, 2017, **7**, 8192–8199.
16 K. Maeda, S. Himeno, T. Osakai, A. Saito and T. Hori, *J. Electroanal. Chem.*, 1994, **364**, 149–154.
17 E. Papaconstantinou and M. T. Pope, *Inorg. Chem.*, 1967, **6**, 1152–1155.
18 B. D. McCarthy and J. L. Dempsey, *Inorg. Chem.*, 2017, **56**, 1225–1231.
19 F. Li and L. Xu, *Dalton Trans.*, 2011, **40**, 4024–4034.
20 J. M. Gómez-Gil, E. Laborda, J. Gonzalez, A. Molina and R. G. Compton, *J. Phys. Chem. C*, 2017, **121**, 26751–26763.
21 H. Guo, D. Goonetilleke, N. Sharma, W. Ren, Z. Su, A. Rawal and C. Zhao, *Cell Rep. Phys. Sci.*, 2020, **1**, 100225.
22 T. J. Thibodeau, A. S. Canney, W. J. DeSisto, M. C. Wheeler, F. G. Amar and B. G. Frederick, *Appl. Catal. A: Gen.*, 2010, **388**, 86–95.
23 M. J. Bezdek, S. Guo and P. J. Chirik, *Science*, 2016, **354**, 730–733.
24 R. G. Agarwal, S. C. Coste, B. D. Groff, A. M. Heuer, H. Noh, G. A. Parada, C. F. Wise, E. M. Nichols, J. J. Warren and J. M. Mayer, *Chem. Rev.*, 2022, **122**, 1–49.
25 C. F. Wise, R. G. Agarwal and J. M. Mayer, *J. Am. Chem. Soc.*, 2020, **142**, 10681–10691.
26 J. J. Warren and J. M. Mayer, *Biochemistry*, 2015, **54**, 1863–1878.
27 P. Mondal, I. Ishigami, E. F. Gérard, C. Lim, S.-R. Yeh, S. P. de Visser and G. B. Wijeratne, *Chem. Sci.*, 2021, **12**, 8872–8883.
28 S. E. Cooney, M. R. A. Walls, E. Schreiber, W. W. Brennessel and E. M. Matson, *J. Am. Chem. Soc.*, 2024, **146**, 2364–2369.
29 S. E. Cooney, E. Schreiber, W. W. Brennessel and E. M. Matson, *Inorg. Chem. Front.*, 2023, **10**, 2754–2765.
30 S. Busbongthong and T. Ozeki, *Bull. Chem. Soc. Jpn.*, 2009, **82**, 1393–1397.
31 E. Coronado, J. R. Galán-Mascarós, C. Giménez-Saiz, C. J. Gómez-García, E. Martínez-Ferrero, M. Almeida, E. B. Lopes, S. C. Capelli and R. M. Llusar, *J. Mater. Chem.*, 2004, **14**, 1867–1872.

Data availability statement:

All experimental data are provided in the ESI.†